HHS Public Access

Author manuscript

Nat Commun. Author manuscript; available in PMC 2015 May 14.

Published in final edited form as:

Nat Commun. ; 5: 5410. doi:10.1038/ncomms6410.

Decreased tumorigenesis in mice with a *Kras* point mutation at C118

Lu Huang[1], **John Carney**[2], **Diana M. Cardona**[2], and **Christopher M. Counter**[*,1,3]

[1]Department of Pharmacology & Cancer Biology, Duke University Medical Center, DUMC-3813 Durham, NC, 27713.

[2]Department of Pathology, Duke University Medical Center, DUMC-3813 Durham, NC, 27713.

[3]Department of Radiation Oncology, Duke University Medical Center, DUMC-3813 Durham, NC, 27713.

Abstract

KRAS, *NRAS*, or *HRAS* genes are mutated to encode an active oncogenic protein in a quarter of human cancers. Redox-dependent reactions can also lead to Ras activation in a manner dependent upon the thiol residue of cysteine 118 (C118). Here, to investigate the effect of mutating this residue on tumorigenesis, we introduce a C118S mutation into the endogenous murine *Kras* allele and expose the resultant mice to the carcinogen urethane, which induces *Kras* mutation-positive lung tumors. We report that $Kras^{+/C118S}$ and $Kras^{C118S/C118S}$ mice develop fewer lung tumors. Although the $Kras^{C118S}$ allele does not appear to affect tumorigenesis when the remaining *Kras* allele is conditionally oncogenic, there is a moderate imbalance of oncogenic mutations favoring the native *Kras* allele in tumors from $Kras^{+/C118S}$ mice treated with urethane. We conclude that the $Kras^{C118S}$ allele impedes urethane-induced lung tumorigenesis.

Introduction

The Ras family of small GTPases, comprised of the *KRAS*, *NRAS*, and *HRAS* genes, are mutated to encode constitutively-active, GTP-bound, oncogenic proteins in upwards of one quarter of all human cancers, which is well established to promote tumorigenesis[1]. Despite the prominent role these genes play in human cancer, the encoded proteins have proven difficult to pharmacologically inhibit[2,3]. As such, it is important to understand how Ras proteins are activated. In this regard, Ras proteins cycle between GDP-bound inactive and GTP-bound active states, the latter being catalyzed by *g*uanine nucleotide *e*xchange *f*actors (GEFs)[4,5]. GEFs are not, however, the only means of activating Ras proteins. Free radical

*Corresponding author (count004@mc.duke.edu)..

Author Contributions

LH and CMC conceived the study. LH performed the experiments. DMC and JC performed histological analysis of lung tumors. All authors contributed to the writing of the manuscript.

Competing Financial Interest

The authors declare no competing financial interests.

oxidants can lead to *S*-nitrosylation or *S*-glutathiolation and activation of Ras in a manner dependent on the thiol residue of cysteine 118 (C118)[6-8]. Accumulating evidence supports the possibility that such redox-dependent reactions with C118 may have cellular consequences. Specifically, an increase in *S*-nitrosylation and activation of Ras can stimulate MAPK signaling[6,9-14], PI3K signaling[15], and/or cell proliferation[16]. Similarly, an increase in *S*-glutathiolation and activation of Ras impacts a variety of signaling pathways in a manner apparently dependent upon C118[17,18]. Finally, reducing the expression of endothelial nitric oxide synthase (eNOS), which catalyzes the production of nitric oxide[19], decreases the levels of *S*-nitrosylated and active Ras as well as xenograft tumor growth in a number of cancer cell lines[20].

Despite accumulating data, the effect of specifically blocking redox-dependent reactions with C118 on the function of endogenous mammalian Ras remains to be explored *in vivo*. This is especially important in terms of cancer, as tumor initiation appears to be incredibly sensitive to the level of activated Ras[21]. Fortunately, there is a very precise separation-of-function mutation that apportions these effects from other functions of Ras. Specifically, substitution of C118 for serine (C118S), a very minor modification in which the thiol residue of this cysteine is replaced with a hydroxyl group, renders Ras completely insensitive to activation by free radical mediated oxidants, with no measureable effect on the protein structure, GTPase activity, intrinsic and GEF-mediated guanine nucleotide dissociation rate, or the ability to bind an effector[6,8,10,12,17,18,22-24]. Thus, here we assess the consequences of introducing the C118S mutation into the endogenous murine *Kras* gene on tumorigenesis *in vivo*, and find a reduction in carcinogen-induced lung tumorigenesis in mice bearing this mutated allele.

Results

Generation of mice with a *Kras^{C118S}* allele

To investigate the effect of mutating C118 on Ras function *in vivo* during tumorigenesis, a targeting vector was created to insert a single point mutation, namely a G353 transversion to C (G353>C) encoding the C118S mutation, into exon 3 of the murine *Kras* gene (Fig. 1a). C118S was chosen because this precise separation-of-function mutation specifically blocks the redox-dependent reactions at this site that lead to Ras activation[6,8,10,12,17,18,22-24]. *Kras* was chosen, as this is the isoform most commonly mutated in human cancers[1]. This vector was electroporated into embryo stem (ES) cells, and cells were selected for resistance to G418 and ganciclovir. Successful recombination events in resistant clones were verified by RT-PCR and sequencing to contain the G353>C transversion in *Kras* (Fig. 1b). One such clone was used to generate a founder *Kras$^{+/C118S(Neo)}$* mouse, the genotype of which was identified by PCR amplification from genomic DNA. A 314 bp product unique to the targeted *Kras$^{C118S(Neo)}$* allele was amplified (Supplementary Fig. 1a) using primers anchored in exon 3 of the *Kras* gene and in the *Neo* gene of the targeting vector (P3 and P4, Fig. 1a and Supplementary Table 4), while a 621 bp product unique to the wild type *Kras* allele was amplified (Supplementary Fig. 1a) using primers anchored in exon 3 and in the adjacent intron (P3 and P5, Fig. 1a and Supplementary Table 4). These mice were crossed with *CMVCre* transgenic mice to induce Cre-mediated recombination between the *loxP* sites

flanking the *Neo* cassette. Successful excision of the *Neo* cassette was identified by PCR amplification of genomic DNA, yielding a 517 bp, instead of a 621 bp product, using primers P3 and P5, as well as by confirming the absence of the aforementioned 314 bp product using primers P3 and P4 (Supplementary Fig. 1b). The presence of *CMVCre* was identified by PCR amplification of genomic DNA using primers (P16 and P17, Supplementary Table 4) designed to generate a 100 bp PCR product unique to this transgene (Supplementary Fig. 1b). *CMVCre;Kras*$^{+/C118S}$ mice identified in this fashion were then crossed with *Kras*$^{+/+}$ mice to generate *Kras*$^{+/C118S}$ mice without *CMVCre* for use in subsequent experiments, again with the desired genotypes confirmed by similar PCR strategies. Finally, *Kras*$^{+/C118S}$ mice were crossed, generating *Kras*$^{+/+}$, *Kras*$^{+/C118S}$, and *Kras*$^{C118S/C118S}$ offspring, the genotype of which were identified by PCR amplification of genomic DNA using the aforementioned primer pair P3 and P5 (Fig. 1a and Supplementary Table 4) that distinguished wild type versus C118S *Kras* alleles by the amplification of a 621 bp versus a 517 bp product (Fig. 1c and Supplementary Fig. 6a).

Characterization of the *Kras*^{C118S} allele

We confirmed that the strategy to introduce the G353>C transversion into the *Kras* gene did not overtly affect alternative splicing of terminal exons 4A and 4B, an important consideration as both splice forms are important for carcinogen-induced lung tumorigenesis[25,26]. Specifically, RT-PCR analysis with primers designed to amplify only *Kras* 4A or only *Kras* 4B detected both versions in lung tissue isolated from *Kras*$^{+/+}$ and *Kras*$^{C118S/C118S}$ mice (Fig. 1d and Supplementary Fig. 6b). Similarly, we confirmed that this alteration of the *Kras* gene did not overtly affect protein expression, given that tumor initiation is sensitive to the level of Ras protein[21]. Specifically, immunoblot analysis revealed no detectable difference in the amount of Kras protein in lung tissue isolated from *Kras*$^{+/+}$ versus *Kras*$^{C118S/C118S}$ mice (Fig. 1e and Supplementary Figs. 2, 6c). Finally, we demonstrate that introducing the C118S mutation into endogenous *Kras* gene can affect the ability of eNOS to stimulate the MAPK pathway. Specifically, mouse embryonic fibroblasts (MEFs) were isolated from two control *Kras*$^{+/+}$ and two experimental *Kras*$^{C118S/C118S}$ embryos and immortalized with the SV40 early region. These four cell lines were then stably infected with a retrovirus encoding no transgene or the S1177D activated mutant version of HA-tagged eNOS[27,28]. Lysates isolated seven independent times from the resultant eight cell lines were then immunoblotted for ectopic eNOS, endogenous Kras, and tubulin, as well as total (T) and phosphorylated (P) Erk1/2. While the normalized levels of P-Erk1/2 varied from experiment to experiment amongst the samples, on average there was a smaller fold increase in the normalized P-Erk1/2 levels upon expression of eNOS^{S1177D} in *Kras*$^{C118S/C118S}$ compared to *Kras*$^{+/+}$ MEFs (0.90±0.14 versus 3.21±0.91, P<0.02, Fig. 2 and Supplementary Fig. 6d). Collectively, we conclude that the single G353>C transversion encoding the desired C118S mutation was successfully knocked into the *Kras* locus with no overt effect on the expression of the resultant gene products.

Kras$^{C118S/C118S}$ mice appear normal

Identification of genotypes of 580 offspring from crossing *Kras*$^{+/C118S}$ mice revealed that there was no statistical difference between the observed frequency versus the expected Mendelian ratio of the three genotypes of *Kras*$^{+/+}$, *Kras*$^{+/C118S}$, and *Kras*$^{C118S/C118S}$ (Chi-

square test, P=0.545, Table 1). *Kras*$^{C118S/C118S}$ mice were also phenotypically indistinguishable from *Kras*$^{+/+}$ mice (Fig. 3a). Weekly weight measurements, beginning at 8 weeks of age and continuing for another 17 weeks, revealed no statistical difference in the weight of either male or female mice between the *Kras*$^{+/+}$ versus *Kras*$^{C118S/C118S}$ genotypes (Fig. 3b,c). The *Kras*$^{-/-}$ genotype is embryonic to neonatal lethal, and is characterized by defective cardiovascular function[29]. As heart defects are a hallmark of defective Kras function, we also compared the heart-to-body weight ratio between *Kras*$^{+/+}$ versus *Kras*$^{C118S/C118S}$ mice, finding no significant difference between the two cohorts (Fig. 3d). Finally, *Kras*$^{+/+}$ mice had a median lifespan of 847 days while *Kras*$^{C118S/C118S}$ mice had a median lifespan of 670 days, but the difference was not significant (Fig. 3e). Collectively, these data indicate that mice with one or more *Kras*^{C118S} alleles do not have any obvious developmental or physiological defects.

Reduced carcinogenesis in mice with a *Kras*^{C118S} allele

To determine the impact of the *Kras*^{C118S} mutation on carcinogenesis, we assessed the effect of treating *Kras*$^{+/+}$, *Kras*$^{+/C118S}$, and *Kras*$^{C118S/C118S}$ mice with the carcinogen urethane (ethyl carbamate), which induces lung tumors characterized by oncogenic Q61R/L mutations in *Kras*[30]. We chose this approach to model a *Kras* mutation-positive cancer spontaneously arising from an environmental insult[30] in the lung, especially given the prevalence of *KRAS* mutations in human lung cancer[31]. As an important note, the *Pas1* locus responsible for the different susceptibilities to urethane-induced tumorigenesis observed amongst inbred strains of mice maps to a region containing six genes, one being *Kras*[32]. Therefore, *Kras*$^{+/C118S}$ mice, which possess the *Kras*^{C118S} allele from the 129S6/SvEvTac background, but the other native *Kras* allele from the C57/BL6 background (introduced during the excision of the *Neo* cassette), were crossed with *Kras*$^{+}$/$^{+}$ mice from the 129S6/SvEvTac background. Resultant *Kras*$^{+/C118S}$ mice were then crossed to generate *Kras*$^{+}$/$^{+}$, *Kras*$^{+/C118S}$, and *Kras*$^{C118S/C118S}$ mice in which both *Kras* alleles originated from a 129S6/SvEvTac background. Cohorts of 27 *Kras*$^{+}$/$^{+}$, 25 *Kras*$^{+/C118S}$, and 25 *Kras*$^{C118S/C118S}$ littermates from multiple breeding pairs were then intraperitoneally injected with urethane at eight weeks of age. Eight months later, mice from all three cohorts were euthanized and lungs removed for analysis.

Comparison of the number and size of visible surface lung lesions revealed that *Kras*$^{+/C118S}$ or *Kras*$^{C118S/C118S}$ mice developed fewer tumors with a smaller average tumor size, resulting in an overall reduction in tumor burden, as defined by the sum of the diameters of all visible surface tumors per mouse, compared to control *Kras*$^{+}$/$^{+}$ mice. There was no statistical difference in tumor number or size between the *Kras*$^{+/C118S}$ and *Kras*$^{C118S/C118S}$ cohorts (Fig. 4a-d and Table 2). Binning tumors based on size, namely small (≤1mm), medium (1-3 mm), or large (≥3mm), revealed a significant shift (Chi-square test, P=0.0014) from larger tumors in *Kras*$^{+}$/$^{+}$ mice to smaller tumors in *Kras*$^{C118S/C118S}$ mice (Table 2). To independently validate these results, one lung from each of the mice in the three cohorts was formalin fixed, paraffin embedded, sectioned, H&E stained, and the type and size of tumors analyzed. Focusing on the most common type of lesion, adenomas were microscopically counted and binned as above as being small, medium, or large. Again, there was a shift to smaller tumors in mice having one or more *Kras*^{C118S} alleles. Specifically, large adenomas

were only detected in *Kras*$^{+/+}$ mice, and these mice also had a higher incidence of adenomas of medium size, while *Kras*$^{+/C118S}$ and *Kras*$^{C118S/C118S}$ mice had a statistically higher incidence of small-sized adenomas (Chi-square test, $P \leq 0.01$, Table 3). Collectively, these data demonstrate that the presence of the *Kras*^{C118S} allele impairs urethane carcinogenesis.

To assess whether there was also an impact on tumor progression, lesions were graded[33] as being *a*typical *a*denomatous *h*yperplasia (AAH), *a*denoma (AD), or *a*deno*c*arcinoma (AC) by histology (Supplementary Fig. 3). This analysis revealed a similar tumor spectrum amongst the three genotypes. Specifically, regardless of the genotype, the majority of the tumors were AD, with only a few AAH and an infrequent number of AC in each group (Supplementary Table 1). AD lesions were further classified[34] into papillary, solid, or mixed solid/papillary subtypes (Supplementary Fig. 3). There was no significant difference in the incidence of solid AD among the three groups, although the *Kras*$^{+/C118S}$ mice appeared to have fewer papillary AD and more mixed solid/papillary AD (Supplementary Table 2). Finally, immunohistochemical analysis of lung lesions in four to six random microscope fields from five mice each having the genotypes *Kras*$^{+/+}$, *Kras*$^{+/C118S}$, or *Kras*$^{C118S/C118S}$ after treatment with urethane did not show any overt difference in the level of Ras signaling, as assessed by P-Erk1/2 or P-Akt immunostaining, or in proliferation, as assessed by Ki67 immunostaining, with the exception of reduced P-Akt in the *Kras*$^{+/C118S}$ cohort (Supplementary Fig. 4a,b). Collectively, these data point towards a negative effect of the *Kras*^{C118S} allele, particularly at the stage of tumor initiation.

Similar tumorigenesis between *Kras*$^{LSL\text{-}G12D/+}$ and *Kras*$^{LSL\text{-}G12D/C118S}$ mice

In the urethane-induced lung tumor model, typically only one *Kra*s allele acquires an oncogenic mutation. While the oncogenic *Kras* allele is well established to promote tumorigenesis, the remaining non-oncogenic allele has actually been found to be tumor suppressive[35]. As such, the observed negative effect of the *Kras*^{C118S} allele on lung tumorigenesis is ostensibly due to the C118S mutation either suppressing the tumorigenic activity of oncogenic *Kras* allele and/or enhancing tumor suppressive effect of the remaining non-oncogenic *Kras* allele. To test the latter possibility, we took advantage of mice with a conditionally oncogenic *LSL-Kras*^{G12D} allele to compare the effect of the remaining *Kras* allele with or without a C118S mutation on lung tumorigenesis. In more detail, infection of lung tissue upon intranasal administration of adenovirus encoding Cre (AdCre) induces recombination of *loxP* sites flanking a transcriptional/translational STOP sequence (*LSL*) upstream of *Kras* harboring a G12D oncogenic mutation, thereby permitting expression of the *Kras*^{G12D} allele, which promotes lung tumorigenesis[36]. Thus, *LSL-Kras*$^{G12D/+}$ mice were crossed with *Kras*$^{+/C118S}$ mice in which both *Kras* alleles were of the 129S6/SvEvTac background. Cohorts of 21 resultant *Kras*$^{LSL\text{-}G12D/+}$ and 17 *Kras*$^{LSL\text{-}G12D/C118S}$ littermates from multiple breeding pairs were treated intranasally with AdCre at eight weeks of age. Four months later mice from both cohorts were euthanized and lungs removed for analysis. Quantification of the number, size, and total burden of visible surface lesions revealed no statistical difference between the two cohorts (Fig. 5a-c). The sizes of these cohorts are powered to detect differences in the number, burden, and size of 1.52, 1.78 mm, and 0.52 mm, respectively. Similarly, microscopic quantification of the number of lesions in H&E stained lung sections from these mice (Supplementary Fig. 5) revealed no significant

difference between these two cohorts (Fig. 5d). Thus, the *Kras*^{C118S} allele does not appear to confer any overt change to the tumor suppressive activity to the non-oncogenic allele in a lung tumor model driven by *Kras*^{G12D}.

Mutational bias against the *Kras*^{C118S} allele

We next tested whether there was a bias of oncogenic mutations induced by urethane in either the native or C118S *Kras* allele in *Kras*$^{+/C118S}$ mice. To this end, RNA was extracted from 65 lung tumors from 20 *Kras*$^{+/C118S}$ mice treated with urethane. *Kras* mRNA was then RT-PCR amplified, cloned, and sequenced to identify the allelic origin (native or C118S) and mutation status (wild type or oncogenic). No oncogenic mutation was detected in either *Kras* allele in 21 tumors, only one allele was recovered in another nine tumors, and a mutation was detected in both alleles in three tumors. As such, these samples were excluded from the analysis. Of the remaining 32 tumors (derived from 15 *Kras*$^{C118S/+}$ mice) in which both *Kras* alleles were recovered and there was an oncogenic mutation in only one of the alleles, 20 tumors had an oncogenic Q61R/L mutation in the native *Kras* allele, while 12 had the mutation in the *Kras*^{C118S} allele (Fig. 6 and Supplementary Table 3). This almost two-fold enrichment in mutations recovered in the native *Kras* allele was significantly different from the expected frequency, assuming the incidence of oncogenic Q61R/L mutations occurring on the native *Kras* and the *Kras*^{C118S} allele was both 50% (Chi-square test, P=0.0455).

The above results suggest a bias against oncogenic mutations in the *Kras*^{C118S} allele. While preliminary experiments revealed that ectopic Kras^{Q61L,C118S} and Kras^{Q61L} behaved rather similarly with regards to signaling, transformation, and oncogene-induced growth arrest, there did appear to be a potential consequence of mutating C118 in the G13D oncogenic mutant background. Specifically, *Kras*$^{C118S/C118S}$ MEFs immortalized with the SV40 early region and transformed with either Kras^{G13D,C118S} or Kras^{G13D} were treated with EGF to stimulate GEF activity, given the potential involvement of GEFs in activating oncogenic Ras proteins[37,38]. Lysates derived three independent times from these two cell lines were then immunoblotted to detect ectopic Kras, endogenous tubulin, as well as total and phosphorylated (P) Erk1/2. On average, this analysis revealed a trend towards a lower normalized P-Erk1/2 level upon EGF treatment in the Kras^{G13D,C118S} compared to Kras^{G13D} transformed MEFs (Fig. 7a,b and Supplementary Fig. 6e). To exclude an involvement of wild type Hras and Nras isoforms[20,39], the *Kras*$^{C118S/C118S}$ genotype was crossed into an *Hras*$^{-/-}$;*Nras*$^{-/-}$ background to generate *Kras*$^{C118S/C118S}$;*Hras*$^{-/-}$;*Nras*$^{-/-}$ MEFs, which were then immortalized with the SV40 early region and transformed with either Kras^{G13D,C118S} or Kras^{G13D}. Based on three independent experiments, on average there was a decrease in the normalized P-Erk1/2 levels upon EGF treatment in the Kras^{G13D,C118S} compared to the Kras^{G13D} transformed *Kras*$^{C118S/C118S}$;*Hras*$^{-/-}$;*Nras*$^{-/-}$ MEFs (Fig. 7c,d and Supplementary Fig. 6f).

Discussion

We report that mutating C118 of endogenous Kras to serine suppressed urethane-induced lung tumorigenesis. We recognize that it is formally possible that the recombined *loxP* sites

introduced into the intron during the generation of the *Kras*^{C118S} allele could underlie this effect rather than the C118S mutation. However, such a possibility seems less likely given that the *Kras*^{C118S} allele yielded both *Kras* 4A and *Kras* 4B transcripts, produced similar levels of protein compared to the native *Kras* allele, and had no observable phenotype in a homozygous setting. The C118S mutation also inhibits the ability of Ras proteins to be activated in the presence of reactive nitrogen or oxygen species[6,8,10,12,17,18,22-24]. Thus, prior research additionally supports a plausible correlation between the mutation of the redox-reactive moiety at the C118 site and the observed reduction in tumorigenicity in mice with one or two *Kras*^{C118S} alleles.

Introducing the C118S mutation into the remaining *Kras* allele in the *LSL-Kras*^{G12D} model of lung cancer had no obvious effect on the number or size of resultant tumors, suggesting that the C118S mutation does not confer any overt change to the tumor suppressive activity of the nononcogenic allele. This does not, however, exclude a role for the C118 in the wild type Kras protein in other settings. Indeed, the C118S mutation in wild type Hras and Nras inhibits the xenograft tumor growth of some cancer cell lines[20]. As such, the effect of mutating this residue may be temporal or context-dependent in cancer, consistent with the highly variable effects of, for example, nitric oxide on tumorigenesis[40]. Nevertheless, extrapolating the results from this experiment, we suggest that the reduction of lung tumors in urethane-treated *Kras*$^{C118S/+}$ or *Kras*$^{C118S/C118S}$ mice may be more related to the oncogenic, rather than remaining non-oncogenic *Kras* allele.

Sequencing analysis suggests a preference of oncogenic mutations in the native compared to the C118S allele in tumors from *Kras*$^{+/C118S}$ mice treated with urethane. It is formally possible that carcinogens cause fewer mutations in the *Kras*^{C118S} allele by some unknown mechanism. However, the C118S is only a point mutation, lies more than 2 kb away and in a completely different exon from where the Q61 oncogenic mutations occur, and is well established to block redox-dependent activation of Ras[6,8,10,12,17,18,22-24]. Thus, we favor a model whereby an oncogenic mutation in the *Kras*^{C118S} allele is less likely to lead to productive tumorigenesis. Accumulating evidence suggests a potential role of GEFs in activating oncogenic Ras proteins[37,38], and in this regard, there was a difference in the ability of EGF to stimulate the MAPK pathway in cells transformed by Kras^{G13D,C118S} versus Kras^{G13D}. However the relationship of NO and urethane tumorigenesis is undoubtedly more complex. NO can be generated from urethane derivatives in the appropriate conditions in vitro[41] and *iNOS* knockout mice are resistant to this carcinogen[42]. As such, the apparent preference of oncogenic mutations in the native compared to the C118S allele of *Kras* awaits a biochemical or cellular explanation. In summary, these results indicate that urethane carcinogenesis is reduced in mice with the *Kras*^{C118S} allele, an effect that may be linked to the oncogenic rather than the native *Kras* version of the gene.

Methods

Plasmids

pBabeNeo-SV40-T/t-Ag (encoding the early region of SV40) was described previously[20,43]. pBabeBleoeNOS^{S1177D}-HA was generated by introducing a mutation resulting in a S1177D amino acid change into C-terminal HA-epitope tagged *eNOS* cDNA[20]. pBabePuroFlag-

Kras^{G13D} was generated by introducing a mutation resulting in a G13D amino acid change into N-terminal FLAG-epitope tagged human *Kras* cDNA[20]. pBabePuroFlag-Kras^{G13D,C118S} was generated by introducing a mutation resulting in a C118S amino acid change into the aforementioned pBabePuroFlag-Kras^{G13D} plasmid.

Animals

All animal experiments were approved by an Institutional Animal Care and Use Committee at Duke University. 129S6/SvEvTac mice were from Taconic. C57BL/6 mice (C57BL/6NJ), CMVCre transgenic mice (B6.C-Tg (CMV-cre)1Cgn/J), and *Kras$^{LSL-G12D}$* transgenic mice (129S/Sv-*Kras^{tm4Tyj}*/J) were obtained from Jackson Laboratory. *Kras^{C118S}* knock-in mice were generated at Transgenic Mouse Facility of Duke Cancer Institute. The described targeting vector (Fig. 1a) was linearized with NotI and electroporated intoW4 ES cells from 129S6/SvEvTac mice, followed by positive selection with G418 and negative selection with ganciclovir. RNA was isolated from individual ES cell clones, and RT-PCR was performed with primers P1 and P2 to amplify *Kras* cDNA (Supplementary Table 4). PCR products were resolved in 2% agarose gels, purified by a gel purification kit (QIAGEN), and sequenced to confirm the *Kras^{C118S}* mutation. One successfully targeted clone was injected into C57BL/6 blastocysts, which were then implanted into pseudo-pregnant females to generate chimeras. Male chimeras were bred with female C57BL/6 mice, and offspring with germline transmission of the *Kras$^{C118S(Neo)}$* allele were identified by PCR of genomic DNA with primer pairs P3+P4 specific for the *Kras^{C118S}* allele and P3+P5 specific for the wild type allele (Supplementary Table 4) as well as direct sequencing of *Kras* RT-PCR products from lung tissue. Male *Kras$^{+/C118S(Neo)}$* mice were bred with female *CMVCre* transgenic mice to excise the *Neo* cassette. The genotypes of offspring were identified by PCR of genomic DNA using the primer pair P3+P5 to identify the wild type *Kras* allele and the *Kras^{C118S}* allele lacking the *Neo* cassette. Absence of the *Neo* cassette was also confirmed with primer pair P3+P4, which does not generate a product when the *Neo* cassette is deleted. *CMVCre;Kras$^{+/C118S}$* mice were then crossed with *Kras$^{+/+}$* mice to generate *Kras$^{+/C118S}$* mice without *CMVCre* for use in all the animal studies. *Kras$^{+/C118S}$* mice were crossed to generate *Kras$^{+/+}$*, *Kras$^{+/C118S}$*, and *Kras$^{C118S/C118S}$* mice, whose genotypes were again identified by PCR of genomic DNA using the primer pair P3+P5. *Kras$^{+/C118S}$* mice were further crossed into *Nras$^{-/-}$*;*Hras$^{-/-}$* background to generate *Nras$^{-/-}$*;*Hras$^{-/-}$*;*Kras$^{+/C118S}$* mice.

Generation of MEFs and cell culture

All the cells were maintained in Dulbecco's modified Eagle's medium (DMEM) supplemented with 10% FBS and incubated at 37°C in a 5% CO_2 incubator. *Kras$^{+/+}$* and *Kras$^{C118S/C118S}$* MEFs were prepared from embryos from *Kras$^{C118S/+}$* females bred with a *Kras$^{C118S/+}$* male. Embryos (E13-E16) were dissected from pregnant *Kras$^{C118S/+}$* females and washed with sterile PBS. The head of each embryo were removed for isolation of genomic DNA and identification of genotypes by PCR using primers P3+P5 as described above. The remaining embryos were cut into pieces in a sterile dish and incubated with 1 ml 0.25% trypsin at 37°C in a 5% CO_2 incubator for 30-45 minutes. The trypsinized cells were then mixed with 10 ml 10% FBS DMEM and incubated at 37°C in a 5% CO_2 incubator for further experiments. *Nras$^{-/-}$*;*Hras$^{-/-}$*;*Kras$^{C118S/C118S}$* MEFs were prepared as above from

embryos from an *Nras*$^{-/-}$;*Hras*$^{-/-}$;*Kras*$^{C118S/+}$ female bred with an *Nras*$^{-/-}$;*Hras*$^{-/-}$;*Kras*$^{C118S/+}$ male. Primary MEF lines were immortalized by stable infection[43] with retroviruses derived from pBabeNeo-SV40-T/t-Ag. In some cases these cells were further stably infected[43] with retroviruses derived from pBabeBleo, pBabeBleo-eNOS^{S1177D}-HA, pBabePuroFlag-Kras^{G13D}, or pBabePuroFlag-Kras^{G13D,C118S}. Where indicated, immortalized MEFs were serum starved by incubating with 0.5% FBS DMEM overnight and harvested the next day. Where indicated, immortalized MEFs were also treated with 100ng/μl Epidermal Growth Factor (Sigma) for 5 minutes at 37°C in a 5% CO_2 incubator before being harvested on ice.

Immunoblot analysis

Cells or lung tissue were lysed with RIPA buffer (1% NP-40, 20 mM Tris pH 8.0, 137 mM NaCl, 10% glycerol, 2mM EDTA) and protein concentrations quantified by Bradford assay (Bio-Rad). Equal amounts of protein lysates (50 μg) were resolved by SDS-PAGE, transferred to a PVDF membrane, and immunoblotted with primary antibodies anti-Kras F234 (Santa Cruz sc-30, diluted 1:200), anti-Flag M2 (Sigma F1804, diluted 1:500), anti-HA (Covance, diluted 1:1000), anti-β-actin (Sigma A2228, diluted 1:10000), anti-β-tubulin (Sigma T5201, diluted 1:2000), anti-Erk1/2 (Santa Cruz sc-94, diluted 1:2000), or anti-P (Thr 202/Tyr 204)-Erk1/2 (Santa Cruz sc-7383, diluted 1:500), followed by incubation with either goat anti-rabbit (Santa Cruz sc-2004, diluted 1:5000) or anti-mouse (Invitrogen G21040, diluted 1:10000) IgG-HRP conjugated secondary antibodiesand detected by ECL (GE healthcare). Bands of targeted protein in scanned images were quantified using Image J software and normalized.

RT-PCR

RNA was extracted from ES cells, lung tissue, or lung tumors with the RNA-BEE reagent according to the manufacture's protocol (Fisher Scientific). 0.5 - 2 μg RNA was reverse transcribed using Omniscript RT kit (QIAGEN) and Oligo dT (QIAGEN) as primers. Resultant cDNA was used as a template to amplify targets of interest using the primers listed in Supplementary Table 4.

Urethane carcinogenesis

Kras$^{+/C118S}$ mice (without CMVCre) were bred with *Kras*$^{+/+}$ mice in 129S6/SvEvTac background. Resultant *Kras*$^{+/C118S}$ mice were then crossed to generate *Kras*$^{+}$/$^{+}$, *Kras*$^{+/C118S}$, and *Kras*$^{C118S/C118S}$ littermates in which both *Kras* alleles originated from a 129S6/SvEvTac background. 25 to 27 male and female mice of each genotype were ultimately compared to detect a measurable difference in tumor parameters between control and experimental cohorts. 38 male and 39 female mice at two months of age were intraperitoneally injected with urethane (1 mg/g body weight)[35]. Weight and behavior were monitored twice weekly starting at three months post-injection. Eight months after injection, mice were euthanized, and lungs were inflated with PBS and harvested for analysis. Lung surface tumors were counted under a dissecting microscope. Tumor diameter was determined using micro-calipers. Mice that reached moribundity endpoints before eight

months were excluded from the final analysis. The investigator was blinded to the genotype when injecting urethane as well as when assessing tumor number and size.

Ad-Cre-induced lung tumorigenesis

Kras$^{+/C118S}$ mice in which both *Kras* alleles originated from a 129S6/SvEvTac background were bred with *LSL-Kras*$^{G12D/+}$ mice to generate *Kras*$^{LSL\text{-}G12D/+}$ and *Kras*$^{LSL\text{-}G12D/C118S}$ mice. 17 to 21 male and female mice of each genotype were ultimately compared to detect a measurable difference in tumor parameters between control and experimental cohorts. 9 male and 29 female mice were infected with 6x10E^6 pfu of AdCre virus at two months of age[36]. Weight and behavior were monitored twice weekly starting at three months post-AdCre. Four months after AdCre administration, mice were euthanized and lungs were inflated with PBS and harvested for analysis. Surface tumors were counted under a dissecting microscope. Tumor diameter was determined using micro-calipers. Mice that reached moribundity endpoints before four months were excluded from the final analysis. The investigator was blinded to the genotype when administrating AdCre as well as when assessing tumor number and size.

Histological analysis

Left lobes of lungs from the indicated mice (*see* above) were fixed in 10% neutral buffered formalin overnight, dehydrated in 70% ethanol, and paraffin embedded. 5 μm-thick sections were cut from each sample, mounted on glass slides, and stained with Hematoxylin and Eosin (H&E). A total of 77 lung sections were reviewed by two pathologists (DMC, JC) who were masked to the study design and blinded to the genotype. The number and type (atypical adenomatous hyperplasia (AAH), adenoma (AD), and/or adenocarcinoma (AC)) of lesions were quantified in each sample. Adenomas were further classified by size (≤1 mm, 1-3 mm or ≥3 mm) and histological subtype (solid, papillary, or mixed solid-papillary)[34].

Immunohistochemistry

Left lobes of lungs from the indicated mice (*see* above) were fixed in 10% neutral buffered formalin overnight, dehydrated in 70% ethanol, and paraffin embedded. 5 μm-thick sections were cut from each sample, mounted on glass slides, and subjected to epitope retrieval and stained with anti-P(Thr 202/Tyr 204)-Erk1/2 (Cell Signaling 4376), anti-P(Ser473)-Akt (Cell Signaling 4060), or anti-Ki67 (Thermo Scientific RM9106) antibodies followed by peroxidase-based detection with Vectastain Elite ABC Kits (Vector Labs) and counterstained with haematoxylin. Photographs were taken of four to six high-power (20X) random fields with tumor areas on an Olympus Vanox S microscope. Images were blinded and tumors were circumscribed in stained tissue images with the freehand selection tool in Image J, and the total area of the tumor in pixels was recorded. Tumor images were copied and pasted to new, blank images and color threshold was applied to determine positive-staining areas, using the same parameters for each tumor image. Areas staining positive by these parameters were selected and the positive staining area in pixels was recorded. The percentage of positive-staining area was calculated by dividing the positive-staining area of the tumor in pixels by the total area of tumors in pixels.

Kras mutation analysis

Lung tumors arising in urethane-treated $Kras^{+/C118S}$ mice (*see* above) were removed with the aid of a dissection microscope. 500 ng of RNA isolated from the tumors were RT-PCR amplified (*see* above) using the primer pair P6+P7 containing HindIII and SacI sites, respectively (Supplementary Table 4). Resultant products were cloned into the HindIII and SacI sites of pBluescript vector (from Addgene), after which 12 positive clones from each ligation reaction were sequenced using T7 promoter (Eton Bioscience) to determine whether the clone corresponded to the native or C118S allele of *Kras*, and whether the clone had an oncogenic mutation (at position G12, G13 and Q61).

Statistical analysis

Data were presented as mean values ± standard error of the mean (SEM). Most statistical analyses were performed with Graphpad Prism 5 software. The two-tailed unpaired student's *t* test was used to compare two groups. The one-way ANOVA plus post-hoc Bonferroni's multiple comparison tests were used to compare three or more groups. The MANOVA test was used to compare mice weight change over time between two groups, while the long-rank test was performed to compare the survival between two groups. The Chi-square test was used to analyze difference in frequency (between the observed vs. the expected or between two groups) based on contingency tables. *P* values < 0.05 were considered significant.

Supplementary Material

Refer to Web version on PubMed Central for supplementary material.

Acknowledgements

We thank the Duke Cancer Institute Mouse Transgenic Facility for aid in generating mice with a $Kras^{C118S}$ allele, Benjamin Lampson for assistance in the design of the targeting vector, Nicole Pershing for technical assistance with lung tumor models, Jianqi Zhang for assistance with statistical analysis, and Sharon Campbell, Aaron Hobbs, Donita Brady, and Matt Crowe for review of the manuscript and/or reagents. This work is supported by NIH grant CA123031 (CMC).

References

1. Pylayeva-Gupta Y, Grabocka E, Bar-Sagi D. RAS oncogenes: weaving a tumorigenic web. Nat. Rev. Cancer. 2011; 11:761–774. [PubMed: 21993244]
2. Downward J. Targeting RAS signalling pathways in cancer therapy. Nat. Rev. Cancer. 2003; 3:11–22. [PubMed: 12509763]
3. Gysin S, Salt M, Young A, McCormick F. Therapeutic strategies for targeting ras proteins. Genes Cancer. 2011; 2:359–372. [PubMed: 21779505]
4. Bos JL, Rehmann H, Wittinghofer A. GEFs and GAPs: critical elements in the control of small G proteins. Cell. 2007; 129:865–877. [PubMed: 17540168]
5. Vigil D, Cherfils J, Rossman KL, Der CJ. Ras superfamily GEFs and GAPs: validated and tractable targets for cancer therapy? Nat. Rev. Cancer. 2010; 10:842–857. [PubMed: 21102635]
6. Lander HM, et al. Redox regulation of cell signalling. Nature. 1996; 381:380–381. [PubMed: 8632794]
7. Raines KW, Bonini MG, Campbell SL. Nitric oxide cell signaling: S-nitrosation of Ras superfamily GTPases. Cardiovas. Res. 2007; 75:229–239.

8. Hobbs GA, Bonini MG, Gunawardena HP, Chen X, Campbell SL. Glutathiolated Ras: characterization and implications for Ras activation. Free Radic. Biol. Med. 2013; 57:221–229. [PubMed: 23123410]
9. Ibiza S, et al. Endothelial nitric oxide synthase regulates N-Ras activation on the Golgi complex of antigen-stimulated T cells. Proc. Natl. Acad. Sci. U.S.A. 2008; 105:10507–10512. [PubMed: 18641128]
10. Lander HM, et al. A molecular redox switch on p21(ras). Structural basis for the nitric oxide-p21(ras) interaction. J. Biol. Chem. 1997; 272:4323–4326. [PubMed: 9020151]
11. Lander HM, Jacovina AT, Davis RJ, Tauras JM. Differential activation of mitogen-activated protein kinases by nitric oxide-related species. J. Biol. Chem. 1996; 271:19705–19709. [PubMed: 8702674]
12. Raines KW, Cao GL, Lee EK, Rosen GM, Shapiro P. Neuronal nitric oxide synthase-induced *S*-nitrosylation of H-Ras inhibits calcium ionophore-mediated extracellular-signal-regulated kinase activity. Biochem. J. 2006; 397:329–336. [PubMed: 16569214]
13. Switzer CH, et al. Ets-1 is a transcriptional mediator of oncogenic nitric oxide signaling in estrogen receptor-negative breast cancer. Breast Cancer Res. 2012; 14:R125. [PubMed: 22971289]
14. Lin YF, Raab-Graham K, Jan YN, Jan LY. NO stimulation of ATP-sensitive potassium channels: Involvement of Ras/mitogen-activated protein kinase pathway and contribution to neuroprotection. Proc. Natl. Acad. Sci. U.S.A. 2004; 101:7799–7804. [PubMed: 15136749]
15. Lee M, Choy JC. Positive feedback regulation of human inducible nitric-oxide synthase expression by Ras protein *S*-nitrosylation. J. Biol. Chem. 2013; 288:15677–15686. [PubMed: 23599434]
16. Batista W, et al. *S*-nitrosoglutathione and endothelial nitric oxide synthase-derived nitric oxide regulate compartmentalized ras *S*-nitrosylation and stimulate cell proliferation. Antioxid. Redox Signaling. 2013; 18:221–238.
17. Adachi T, et al. *S*-glutathiolation of Ras mediates redox-sensitive signaling by angiotensin II in vascular smooth muscle cells. J. Biol. Chem. 2004; 279:29857–29862. [PubMed: 15123696]
18. Clavreul N, et al. S-glutathiolation by peroxynitrite of p21ras at cysteine-118 mediates its direct activation and downstream signaling in endothelial cells. FASEB J. 2006; 20:518–520. [PubMed: 16415107]
19. Dudzinski DM, Igarashi J, Greif D, Michel T. The regulation and pharmacology of endothelial nitric oxide synthase. Annu. Rev. Pharmacol. Toxicol. 2006; 46:235–276. [PubMed: 16402905]
20. Lim KH, Ancrile BB, Kashatus DF, Counter CM. Tumour maintenance is mediated by eNOS. Nature. 2008; 452:646–649. [PubMed: 18344980]
21. Sarkisian CJ, et al. Dose-dependent oncogene-induced senescence in vivo and its evasion during mammary tumorigenesis. Nat. Cell Biol. 2007; 9:493–505. [PubMed: 17450133]
22. Heo J, Campbell SL. Mechanism of p21Ras *S*-nitrosylation and kinetics of nitric oxide-mediated guanine nucleotide exchange. Biochemistry. 2004; 43:2314–2322. [PubMed: 14979728]
23. Mott HR, Carpenter JW, Campbell SL. Structural and functional analysis of a mutant Ras protein that is insensitive to nitric oxide activation. Biochemistry. 1997; 36:3640–3644. [PubMed: 9132016]
24. Williams JG, Pappu K, Campbell SL. Structural and biochemical studies of p21Ras *S*-nitrosylation and nitric oxide-mediated guanine nucleotide exchange. Proc. Natl. Acad. Sci. U.S.A. 2003; 100:6376–6381. [PubMed: 12740440]
25. Patek CE, et al. Mutationally activated K-ras 4A and 4B both mediate lung carcinogenesis. Exp. Cell Res. 2008; 314:1105–1114. [PubMed: 18062963]
26. To MD, et al. Kras regulatory elements and exon 4A determine mutation specificity in lung cancer. Nat. Genet. 2008; 40:1240–1244. [PubMed: 18758463]
27. Dimmeler S, et al. Activation of nitric oxide synthase in endothelial cells by Akt-dependent phosphorylation. Nature. 1999; 399:601–605. [PubMed: 10376603]
28. Fulton D, et al. Regulation of endothelium-derived nitric oxide production by the protein kinase Akt. Nature. 1999; 399:597–601. [PubMed: 10376602]
29. Koera K, et al. K-ras is essential for the development of the mouse embryo. Oncogene. 1997; 15:1151–1159. [PubMed: 9294608]

30. You M, Candrian U, Maronpot RR, Stoner GD, Anderson MW. Activation of the Ki-ras protooncogene in spontaneously occurring and chemically induced lung tumors of the strain A mouse. Proc. Natl. Acad. Sci. U.S.A. 1989; 86:3070–3074. [PubMed: 2654935]
31. Ding L, et al. Somatic mutations affect key pathways in lung adenocarcinoma. Nature. 2008; 455:1069–1075. [PubMed: 18948947]
32. Manenti G, et al. Haplotype sharing suggests that a genomic segment containing six genes accounts for the pulmonary adenoma susceptibility 1 (Pas1) locus activity in mice. Oncogene. 2004; 23:4495–4504. [PubMed: 15064703]
33. Stathopoulos GT, et al. Epithelial NF-kappaB activation promotes urethane-induced lung carcinogenesis. Proc. Natl. Acad. Sci. U.S.A. 2007; 104:18514–18519. [PubMed: 18000061]
34. Avanzo JL, et al. Increased susceptibility to urethane-induced lung tumors in mice with decreased expression of connexin43. Carcinogenesis. 2004; 25:1973–1982. [PubMed: 15166089]
35. Zhang Z, et al. Wildtype Kras2 can inhibit lung carcinogenesis in mice. Nat.Genet. 2001; 29:25–33. [PubMed: 11528387]
36. Jackson EL, et al. Analysis of lung tumor initiation and progression using conditional expression of oncogenic K-ras. Genes Dev. 2001; 15:3243–3248. [PubMed: 11751630]
37. Hocker HJ, et al. Andrographolide derivatives inhibit guanine nucleotide exchange and abrogate oncogenic Ras function. Proc. Natl. Acad. Sci. U.S.A. 2013; 110:10201–10206. [PubMed: 23737504]
38. Huang H, et al. Oncogenic K-Ras requires activation for enhanced activity. Oncogene. 2014; 33:532–535. [PubMed: 23334325]
39. Jeng HH, Taylor LJ, Bar-Sagi D. Sos-mediated cross-activation of wild-type Ras by oncogenic Ras is essential for tumorigenesis. Nat. Commun. 2012; 3:1168. [PubMed: 23132018]
40. Fukumura D, Kashiwagi S, Jain RK. The role of nitric oxide in tumour progression. Nat.Rev. Cancer. 2006; 6:521–534. [PubMed: 16794635]
41. Sakano K, Oikawa S, Hiraku Y, Kawanishi S. Metabolism of carcinogenic urethane to nitric oxide is involved in oxidative DNA damage. Free Radic. Biol. Med. 2002; 33:703–714. [PubMed: 12208357]
42. Kisley LR, et al. Genetic ablation of inducible nitric oxide synthase decreases mouse lung tumorigenesis. Cancer Res. 2002; 62:6850–6856. [PubMed: 12460898]
43. O'Hayer KM, Counter CM. A genetically defined normal human somatic cell system to study ras oncogenesis in vivo and in vitro. Methods Enzymol. 2006; 407:637–647. [PubMed: 16757358]

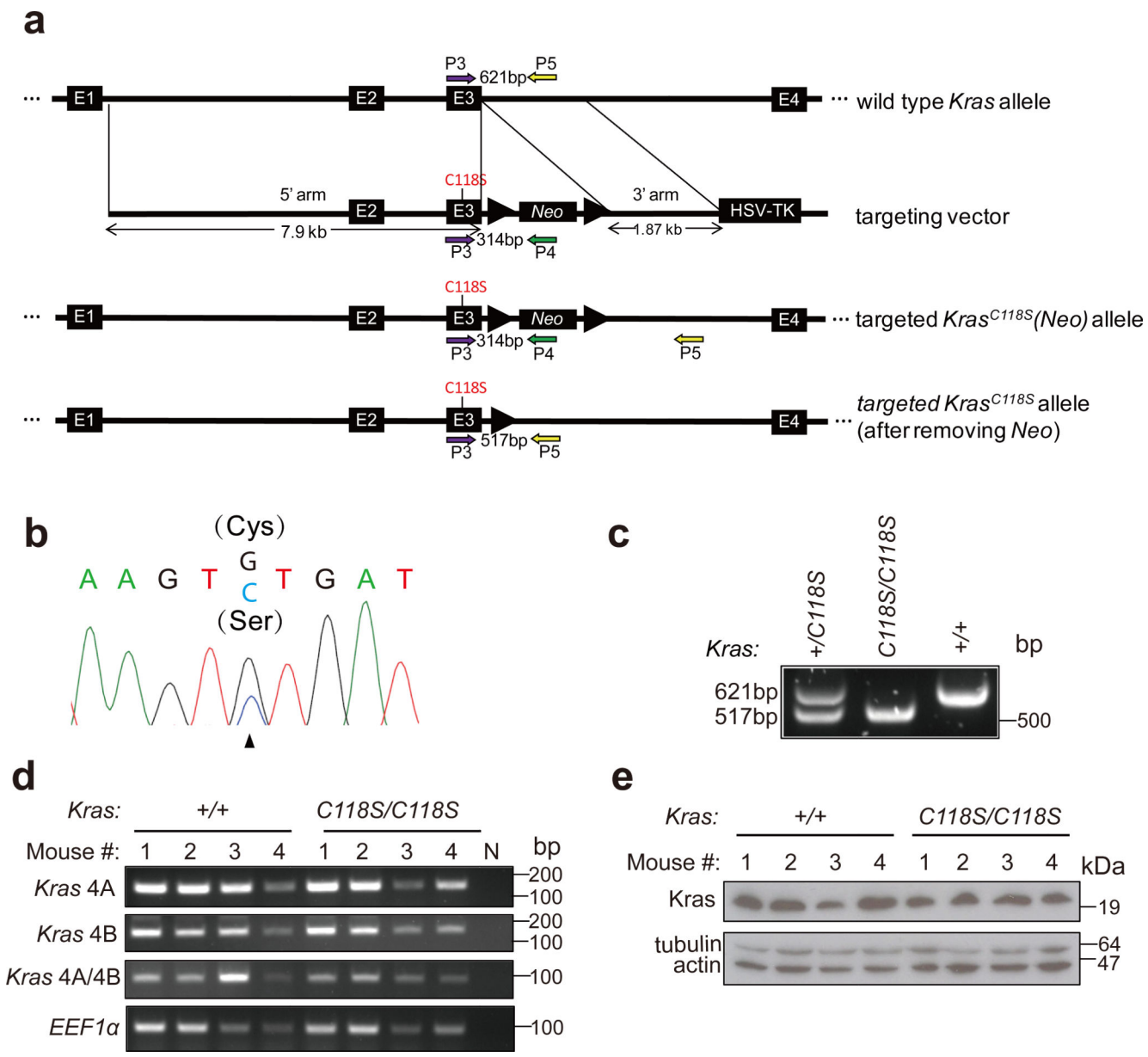

Figure 1. Generation of mice with a *Kras*^{C118S} allele

(**a**) Schematic representation of homologous recombination (thin black lines) between the endogenous wild type *Kras* gene (E-numbered black boxes: exons, thick black lines: introns) and the *Kras*^{C118S} targeting vector (*Neo*: *Neo* selection marker; thick arrows: *loxP* recombination sites; HSV-TK: HSV promoter-driven thymidine kinase negative selection marker) as well as the resultant successfully targeted *Kras*^{C118S} knock-in allele before and after Cre-mediated recombination of the flanking *loxP* sites to excise the *Neo* selection marker. Colored arrows: PCR primers used in genotyping. (**b**) Sequencing chromatogram of RT-PCR amplified *Kras* mRNA from a successfully targeted ES cell clone identifying the wild type (G) and mutated (C) nucleotide at position 353 that changes the cysteine 118 codon to serine. (**c**) PCR amplification using the primer pair P3+P5 of genomic DNA from offspring of the indicated genotypes from crossing *Kras*$^{+/C118S}$ mice. (**d**) RT-PCR

amplification of *Kras* mRNA from the lungs of four $Kras^{+/+}$ mice and four $Kras^{C118S/C118S}$ mice (numbered 1, 2, 3 and 4) using primer pairs specific for the indicated *Kras* splice variants (*see* Supplementary Table 4). N: no DNA as a negative control reaction. *EEF1α*: loading control. (**e**) Immunoblot of lysates isolated from the lungs of four $Kras^{+/+}$ mice and four $Kras^{C118S/C118S}$ mice (numbered 1, 2, 3 and 4) with an anti-Kras antibody. Tubulin and actin: loading controls.

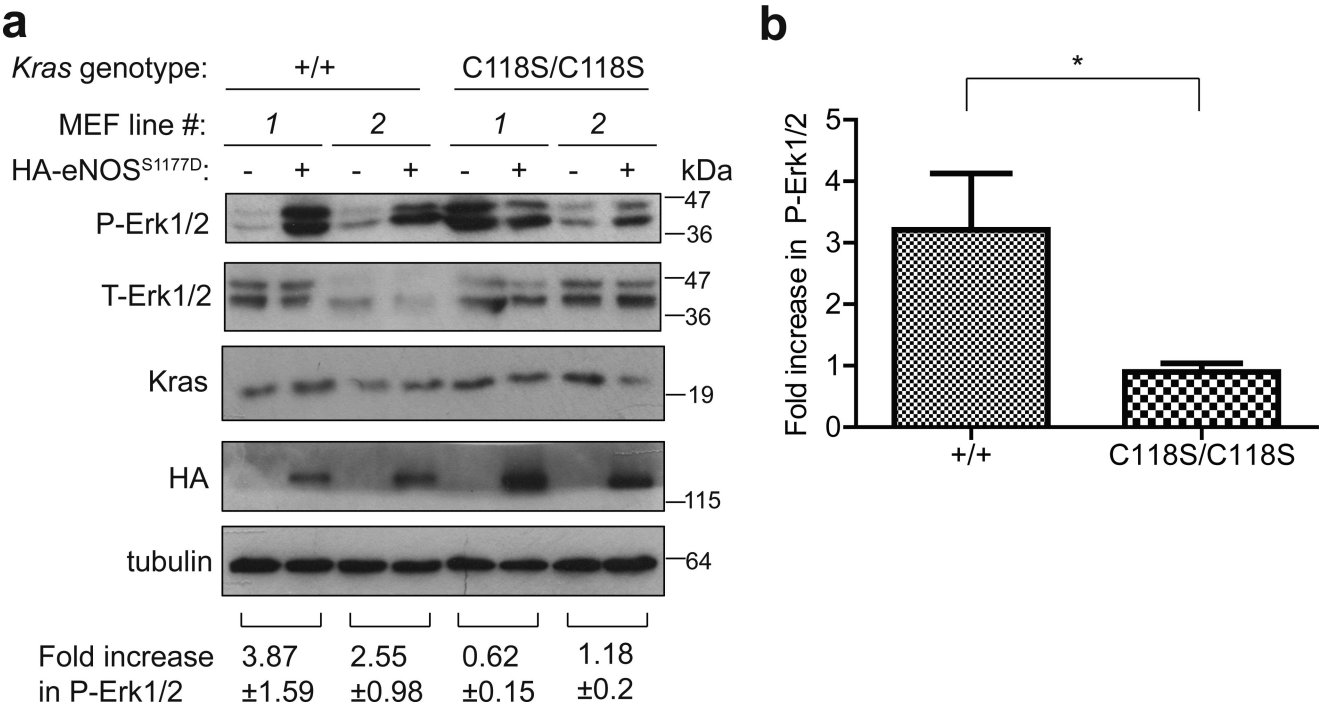

Figure 2. Reduced increase in P-Erk1/2 levels in *Kras*$^{C118S/C118S}$ MEFs upon expressing activated eNOS

(**a**) Immunoblot of HA-tagged ectopic eNOS, endogenous Kras, and tubulin, as well as total (T) and phosphorylated (P) Erk1/2 from two *Kras*$^{+/+}$ and two *Kras*$^{C118S/C118S}$ SV40-immortalized MEF cell lines in the absence or presence of HA-eNOS^{S11777D}. Bottom: Mean ± SEM of the indicated fold increase in P-Erk1/2 (normalized to T-Erk1/2) from immunoblot analysis of lysates derived seven independent times. (**b**) Mean ± SEM fold increase in P-Erk1/2 levels (normalized to T-Erk1/2) upon expression of eNOS^{S1177D} from lysates derived seven independent times from the two *Kras*$^{+/+}$ (+/+) or two *Kras*$^{C118S/C118S}$ (C118S/C118S) SV40-immortalized MEF cell lines. *: $P<0.05$, as determined by two-tailed unpaired Student's *t* test.

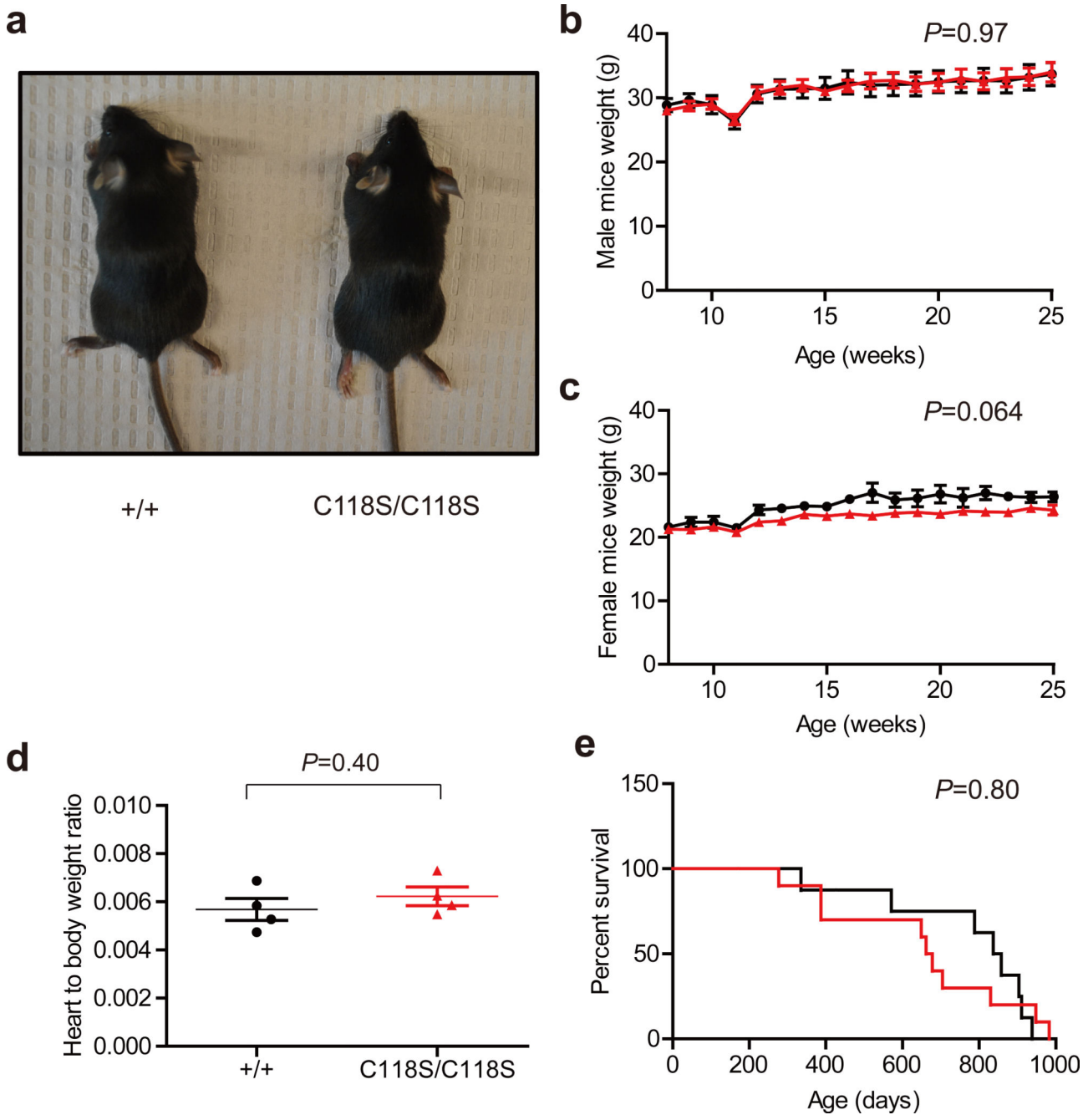

Figure 3. ***Kras*$^{C118S/C118S}$ mice have no overt phenotypes**

(**a**) Photograph of a *Kras*$^{+/+}$ (+/+) and *Kras*$^{C118S/C118S}$ (C118S/C118S) adult mouse at three weeks of age. (**b, c**) Mean body weight ± SEM of (●) *Kras*$^{+/+}$ versus (▲) *Kras*$^{C118S/C118S}$ (**b**) male (*n*=6 versus 5) and (**c**) female mice (*n*= 4 versus 5) from 8 to 25 weeks of age. (**d**) Mean heart to body weight ratio ± SEM of four week old *Kras*$^{+/+}$ (+/+) versus *Kras*$^{C118S/C118S}$ (C118S/C118S) mice (*n*=4). (**e**) Kaplan-Meier survival curves of *Kras*$^{+/+}$ (black line, *n*=8) versus *Kras*$^{C118S/C118S}$ (red line, *n*=10) mice. *P* value was determined by MANOVA test (**b, c**), two-tailed unpaired Student's *t* test (**d**) and long-rank test (**e**).

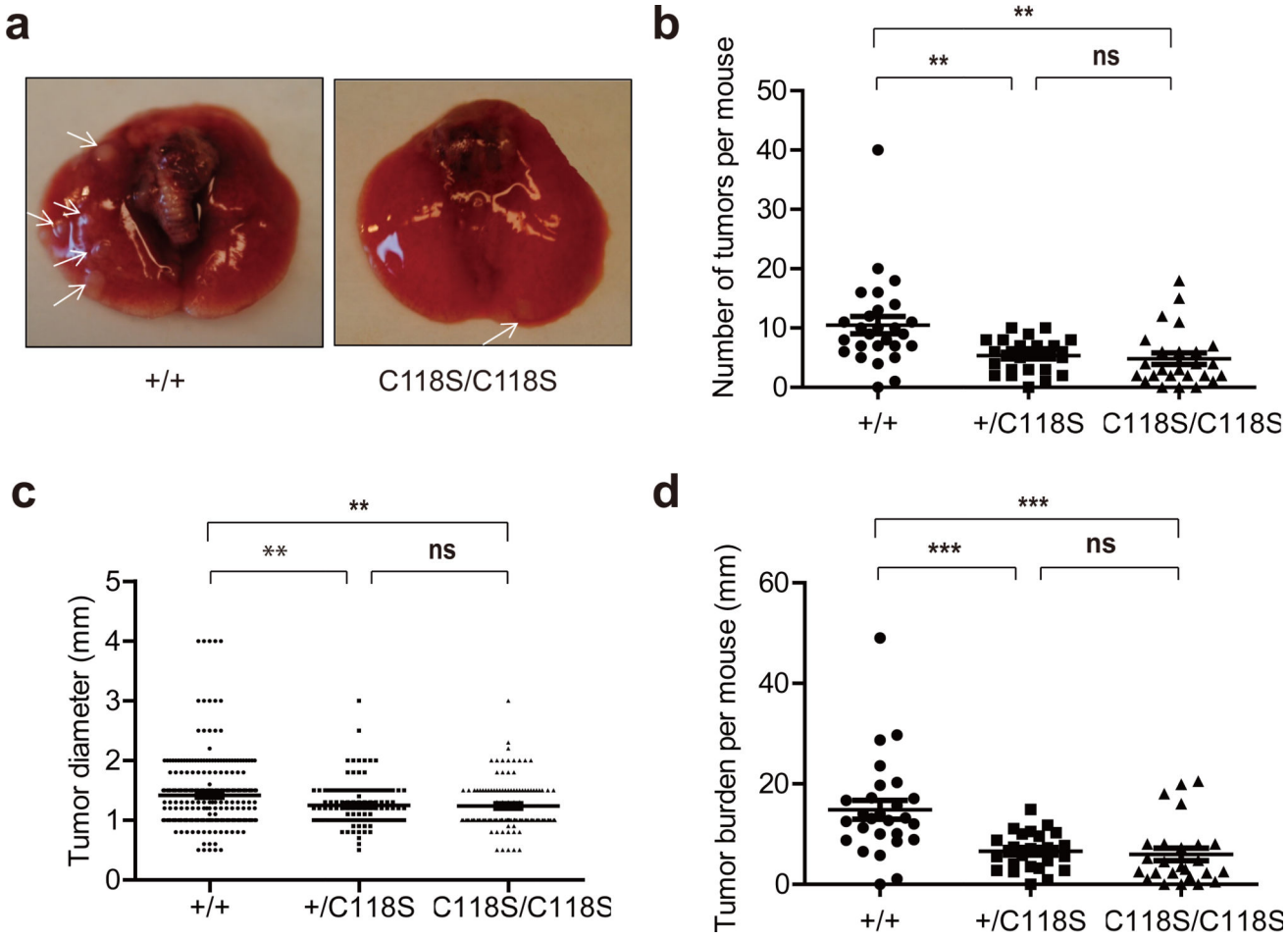

Figure 4. Decreased urethane-induced lung tumorigenesis in mice with a *Kras*^{C118S} allele

(**a**) Visible lesions (arrows) of lungs from one *Kras*$^{+/+}$ (+/+) and one *Kras*$^{C118S/C118S}$ (C118S/C118S) mouse eight months after treatment with urethane. (**b**) Number of visible surface tumor lesions per mouse, (**c**) diameter of each visible surface tumor lesion and, (**d**) tumor burden, as defined by the sum of the diameters of all visible surface tumor lesions per mouse, from *Kras*$^{+/+}$ (+/+, 27 mice, 285 visible surface tumors), *Kras*$^{+/C118S}$ (+/C118S, 25 mice, 132 visible surface tumors), and *Kras*$^{C118S/C118S}$ (C118S/C118S, 25 mice, 121 visible surface tumors) mice eight months after treatment with urethane. Bars: mean ± SEM. ns: non-significant ($P>0.05$), **$P<0.01$ and ***$P<0.001$, as determined using one-way ANOVA plus post-hoc Bonferroni's multiple comparison test.

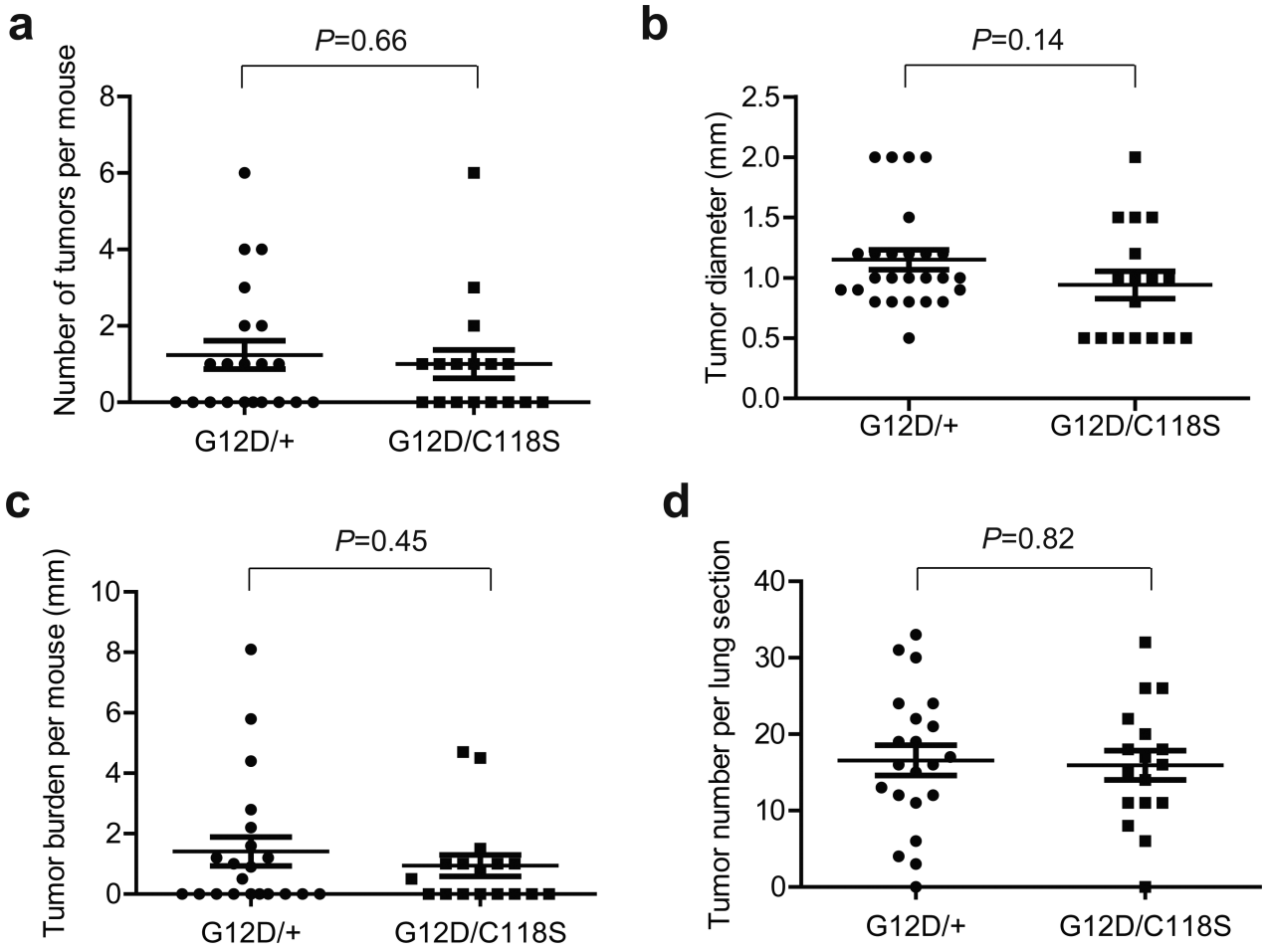

Figure 5. ***Kras*^{G12D}-driven lung tumorigenesis is similar when the remaining *Kras* allele is wild type or C118S**

(**a**) Number of visible surface tumor lesions per mouse, (**b**) diameter of each visible surface tumor lesion, (**c**) tumor burden, as defined by the sum of the diameters of all visible surface tumor lesions per mouse, and (**d**) number of lesions detected in each H&E stained section from *Kras*$^{LSL\text{-}G12D/+}$ (G12D/+, 21 mice, 26 visible surface tumors) versus *Kras*^{LSL} *G12D/C118S* (G12D/C118S, 17 mice, 17 visible surface tumors) mice four months after intranasal administration of AdCre. Bars: mean ± SEM. *P* values were determined using two-tailed unpaired Student's *t*-test.

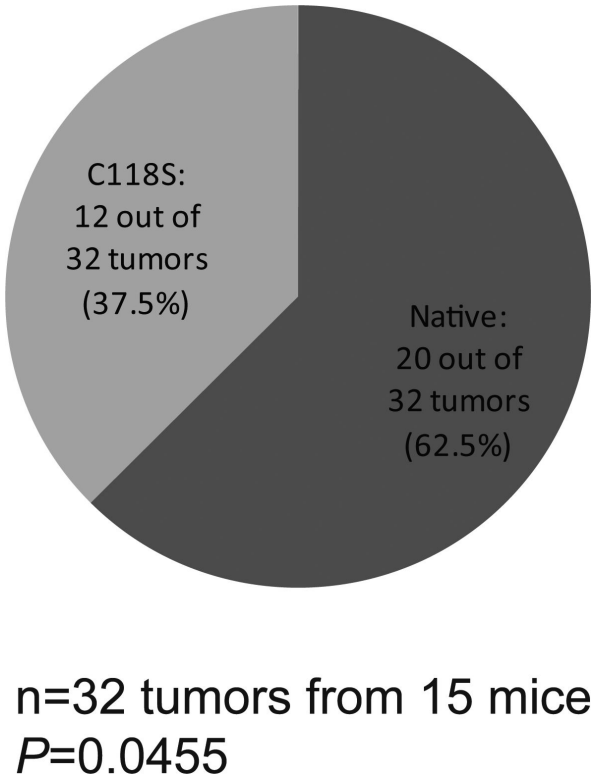

Figure 6. Oncogenic Q61 mutations occur preferentially on the native *Kras* allele

Pie chart of the number and percent of Q61R/L oncogenic mutations found in the native versus the C118S *Kras* allele, as determined by RT-PCR amplification and sequencing of *Kras* mRNA isolated from 32 lung lesions from 15 $Kras^{+/C118S}$ mice eight months after treatment with urethane. *P* value was determined using the Chi-square test to compare the difference between the observed and the expected frequency.

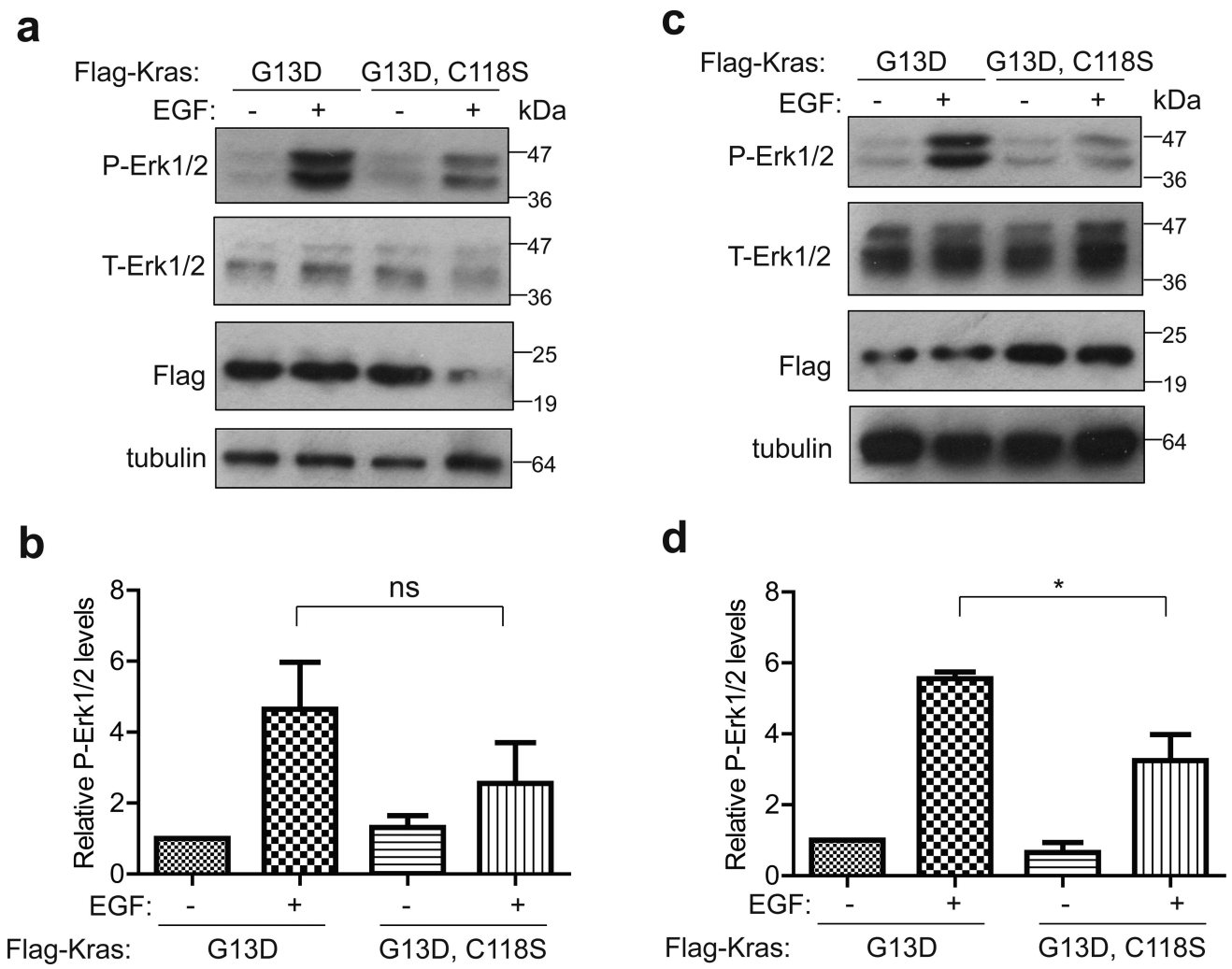

Figure 7. Reduced increase in P-Erk1/2 levels in MEFs transformed with Kras^{G13D,C118S} upon EGF treatment

Immunoblot of Flag-tagged ectopic Kras, tubulin, as well as total (T) and phosphorylated (P) Erk1/2 from (**a**) *Kras$^{C118S/C118S}$* or (**c**) *Nras$^{-/-}$;Hras$^{-/-}$;Kras$^{C118S/C118S}$* MEFs immortalized with the SV40 early region and transformed with either Flag-Kras^{G13D} or Flag-Kras^{G13D,C118S} in the absence or presence of EGF stimulation. (**b**, **d**) Mean ± SEM of P-Erk1/2 levels (normalized to T-Erk1/2) from three independent experiments using lysates from (**b**) *Kras$^{C118S/C118S}$* or (**d**) *Nras$^{-/-}$;Hras$^{-/-}$;Kras$^{C118S/C118S}$* MEFs immortalized with the SV40 early region and transformed with either Flag-Kras^{G13D} or Flag-Kras^{G13D,C118S} in the absence or presence of EGF stimulation. ns: non-significant (P>0.05). *: P<0.05, as determined using one-way ANOVA plus post-hoc Bonferroni's multiple comparison test.

Table 1

Expected and observed frequencies of offspring from crossing *Kras*$^{+/C118S}$ mice.

***Kras* Genotype**	**Expected Frequency**	**Observed Frequency**
+/+	25% (145/580)	26.72% (155/580)
+/C118S	50% (290/580)	47.93% (278/580)
C118S/C118S	25% (145/580)	25.34% (147/580)

Table 2

Quantification of surface lung tumors from urethane-treated mice.

Kras genotype	Number of mice	Tumor incidence	Mean ± SEM tumors per lung	Total number of tumors	Tumor incidence by size (mm)		
					≤1	1 – 3	≥3
+/+	27	96.3%	10.52 ± 1.46	285	37.5%	58.9%	3.5%
+/C118S	25	96.0%	5.36 ± 0.56	132	41.7%	57.6%	0.76%
C118S/C118S	25	88.0%	4.84 ± 0.95	121	56.2%	43.0%	0.83%

Table 3

Histological quantification of lung adenomas from urethane-treated mice.

Kras genotype	Number of lung sections	Adenoma incidence	Mean ± SEM adenomas per section	Total number of adenomas	Adenoma incidence by size (mm)		
					≤1	1 – 3	≥3
+/+	27	85.2%	2.52 ± 0.35	68	52.9%	41.2%	5.9%
+/C118S	25	80.0%	1.92 ± 0.26	48	87.5%	12.5%	0 %
C118S/C118S	25	80.0%	1.64 ± 0.38	41	80.5%	19.5%	0%